ELSEVIER

NeuroImage

www.elsevier.com/locate/ynimg
NeuroImage 28 (2005) 720 – 737

Removal of FMRI environment artifacts from EEG data using optimal basis sets

R.K. Niazy,[a,b,*] C.F. Beckmann,[a] G.D. Iannetti,[a,c] J.M. Brady,[b] and S.M. Smith[a]

[a]*University of Oxford, Centre for Functional MRI of the Brain (FMRIB), John Radcliffe Hospital, Headington, Oxford OX3 9DU, UK*
[b]*Department of Engineering Science, University of Oxford, Oxford, UK*
[c]*Department of Human Anatomy and Genetics, University of Oxford, Oxford, UK*

Received 9 April 2005; revised 8 June 2005; accepted 23 June 2005
Available online 16 September 2005

The combination of functional magnetic resonance imaging (FMRI) and electroencephalography (EEG) has received much recent attention, since it potentially offers a new tool for neuroscientists that makes simultaneous use of the strengths of the two modalities. However, EEG data collected in such experiments suffer from two kinds of artifact. First, gradient artifacts are caused by the switching of magnetic gradients during FMRI. Second, ballistocardiographic (BCG) artifacts related to cardiac activities further contaminate the EEG data. Here we present new methods to remove both kinds of artifact. The methods are based primarily on the idea that temporal variations in the artifacts can be captured by performing temporal principal component analysis (PCA), which leads to the identification of a set of basis functions which describe the temporal variations in the artifacts. These basis functions are then fitted to, and subtracted from, EEG data to produce artifact-free results. In addition, we also describe a robust algorithm for the accurate detection of heart beat peaks from poor quality electrocardiographic (ECG) data that are collected for the purpose of BCG artifact removal. The methods are tested and are shown to give superior results to existing methods. The methods also demonstrate the feasibility of simultaneous EEG/FMRI experiments using the relatively low EEG sampling frequency of 2048 Hz.

Keywords: Simultaneous EEG/FMRI; Gradient artifacts; Ballistocardiographic artifacts; Principal component analysis (PCA)

Introduction

Functional neuroimaging techniques such as positron emission tomography (PET) and functional magnetic resonance imaging (FMRI) have made it possible to map specific areas of the brain that are involved in carrying out tasks of differing complexities. However, such techniques measure brain activity indirectly, i.e., they detect a secondary effect of brain activation rather than the neural activity itself. Furthermore, although such imaging modalities provide good spatial localization, they suffer from relatively low temporal sampling frequency. Electrophysiological mapping methods such as electroencephalography (EEG) and magnetoencephalography (MEG) measure brain electrical activity directly, and in real time, but suffer from spatial blurring of activation. This has encouraged the neuroimaging community to investigate multimodal imaging in order to combine the strengths of the individual techniques. In particular, the simultaneous combination of FMRI and EEG has received recent attention. Initial studies aimed to demonstrate the safety, potential and data quality possible using this technique (Ives et al., 1993; Lemieux et al., 1997; Krakow et al., 2000; Goldman et al., 2000). Subsequently, the use of simultaneous EEG and FMRI has been used to study the generators of the alpha rhythm (Goldman et al., 2002; Laufs et al., 2003; Moosmann et al., 2003; Niazy et al., 2004), event-related brain responses (Bonmassar et al., 1999; Kruggel et al., 2000; Liebenthal et al., 2003), brain activation during different sleep stages (Czisch et al., 2002; Liebenthal et al., 2003) and epileptic activities (Seeck et al., 2001; Krakow et al., 2001; Lemieux et al., 2001; Iannetti et al., 2002; Bénar et al., 2003).

Common to all simultaneous EEG and FMRI experiments, however, are the MRI environment artifacts that contaminate EEG data. There are two kinds of MRI environment artifact. The first kind is the gradient (or imaging) artifact caused by the switching of the magnetic field gradients (Felblinger et al., 1999; Allen et al., 2000). The second kind is the ballistocardiographic (BCG) artifact, which is caused by heart-related blood and electrode movements inside the static magnetic field of the MRI scanner (Allen et al., 1998; Bonmassar et al., 2002), regardless of whether or not MR scanning is being performed. In this paper, we briefly discuss these artifacts, review some of the methods previously proposed to remove them and then propose new methods for their removal. Additionally, a companion paper by Iannetti et al. (this issue) further validates our methods by applying them to simultaneous

* Corresponding author. University of Oxford, Centre for Functional MRI of the Brain (FMRIB), John Radcliffe Hospital, Headington, Oxford OX3 9DU, UK. Fax: +44 1865 222717.
E-mail address: rami@fmrib.ox.ac.uk (R.K. Niazy).
Available online on ScienceDirect (www.sciencedirect.com).

1053-8119/$ - see front matter © 2005 Elsevier Inc. All rights reserved.
doi:10.1016/j.neuroimage.2005.06.067

laser-evoked potentials (LEPs) and FMRI experiments and demonstrating the quality of the acquired data. In the remainder of this section, more detailed information is given about the different kinds of artifact, current methods for their removal, as well as a summary of our proposed methods. Following the Introduction, the Methods section details our proposed algorithms. This is followed by the Validation section, which will describe how the algorithms were tested. Results and Discussion will then follow.

Gradient artifact

During MR imaging, the magnetic field inside the MRI scanner continuously changes as a result of the switching of the magnetic field gradients. The gradients change according to the imaging sequence being used. In an echo planar imaging (EPI) sequence typically used in FMRI, gradient switching is repeated each time a new slice is collected, resulting in artifacts that repeat with the collection of each new FMRI slice. The amplitude of such artifact can be 100 times greater than the EEG signal and its frequency content overlaps that of the EEG, thus gradient artifacts cannot be simply filtered out. The artifact shape and amplitude varies from one EEG channel to another depending on the location of the electrodes and the wire connections. For more details, see Hoffmann et al. (2000), Anami et al. (2003), Garreffa et al. (2003).

Different approaches have been proposed to remove gradient artifacts from biological signals collected during MRI scanning. Hoffmann et al. (2000) proposed a frequency domain method, where the amplitude and phase of the data were set to zero at frequencies matching an artifact power spectrum template. However, this approach suffers from the typical 'ringing' effect common to such frequency domain filters (Bénar et al., 2003). The most used method is average artifact subtraction (Allen et al., 2000; Bénar et al., 2003). This utilizes the repetitiveness of the artifact to form an average artifact template, which is then subtracted from the EEG data. The efficacy of this approach has been demonstrated in the literature (Allen et al., 2000; Bénar et al., 2003; Salek-Haddadi et al., 2003), though a number of quality and practicality issues still remain. Firstly, some residual artifacts remain on some channels. Allen et al. (2000) proposed the use of adaptive noise cancellation (ANC) to remove these residuals; however, this approach does not remove all residual artifacts. Secondly, in order to minimize the residuals, a high sampling frequency is needed. From our experience, some unsatisfactory results are obtained from commercial implementation of this algorithm even at sampling rates of 10 kHz. However, even if better quality data were to be achieved at such high sampling rates, the amount of generated data (especially in high electrode density experiments) limits the length of the experiments and causes practical problems when the data need to be analyzed using third party software such as Matlab® (The MathWorks, Inc., MA, USA).

Fig. 1 shows an example of the gradient artifacts in EEG data and their origin. After subtraction of the average artifact, some residuals remain, which result in sharp deflection in the data after low-pass filtering. This is mainly due to the inaccuracy of the artifact template being subtracted. This inaccuracy is partly caused by the fact that the MRI machine and the EEG system are typically driven by separate clocks, which means that the artifact is not always sampled at exactly the same location. This introduces a slight variation in the shape of the artifact from one slice to another. Also, the average template calculation and subtraction processes are usually dependent on the triggers received from the MRI machine that indicate the start of each artifact segment. The location of these triggers is often slightly inconsistent from one segment to another, which causes a temporal jitter in the onset of the different artifact segments and thus degrades the accuracy of the calculated template. These problems are exacerbated if the sampling frequency is decreased.

In this paper, we propose a new method for the removal of gradient artifacts; FMRI artifact slice template removal (FASTR). In FASTR, a unique artifact template for each slice artifact in each EEG channel is constructed and then subtracted. Each slice template is constructed as the local moving average plus a linear combination of basis functions that describe the variation of residuals. The basis functions are derived by performing temporal principal component analysis (PCA) on the artifact residuals and selecting the dominant components to serve as a basis set. This technique is demonstrated to be superior to imaging artifact reduction (IAR) (Allen et al., 2000) and applicable at a sampling rate as low as 2048 Hz.

Recent independent work by Negishi et al. (2004) has proposed a similar approach to ours. In contrast to our approach, Negishi's work requires the collection of extra EEG data without scanning to serves as a reference. This could well introduce a number of problems, as it assumes the two data sets differ only in the introduction of the gradient artifacts. However, their method utilizes all estimated principal components (rather than the strongest few) and has the advantage of automatically weighting each component depending on its projection on both the contaminated and clean data; Negishi's use of PCA is fairly different and, to an extent, complementary to what we have developed. More discussion of the differences between the two approaches is given later.

Ballistocardiographic artifacts

The BCG artifact is a distortion in the EEG data caused by cardiac-related activities. In a normal, ideal EEG environment it is usually caused by an electrode being directly above a pulsating scalp vessel, and the problem can be avoided by changing the electrode position. Inside the MRI magnet, this problem is greatly magnified. Causes and characteristics of the BCG artifact have been described in the literature (Allen et al., 1998; Bonmassar et al., 2002), and in general it is caused by electrode movement due to pulsatile scalp and blood movement related to the cardiac cycle. This movement of electrodes and conductive blood inside the magnetic field induces the artifacts (Allen et al., 1998). The magnitude of the BCG artifact may be as much as 200 μV at 1.5 T (3–4 times that of the EEG) (Allen et al., 1998), it is spread throughout the heart beat period and it can be observed across the scalp (Allen et al., 1998), although its magnitude and shape can vary considerably from one EEG channel to another. In contrast to the imaging artifact, although the basic shape of the BCG artifact is similar from one occurrence to the next in any single EEG channel, there exists considerable variation in the artifact shape, amplitude and scale over time.

Several approaches have been proposed to remove the BCG artifact. Adaptive filtering has been proposed by Bonmassar et al. (2002): a piezoelectric sensor was used to generate a reference BCG signal, which was then used to filter out BCG contributions from the EEG. This method is computationally expensive, requires the use of an extra sensor and assumes that no EEG correlated information is present in the sensor signal. Spatial PCA and independent component analysis (ICA) filters have also been

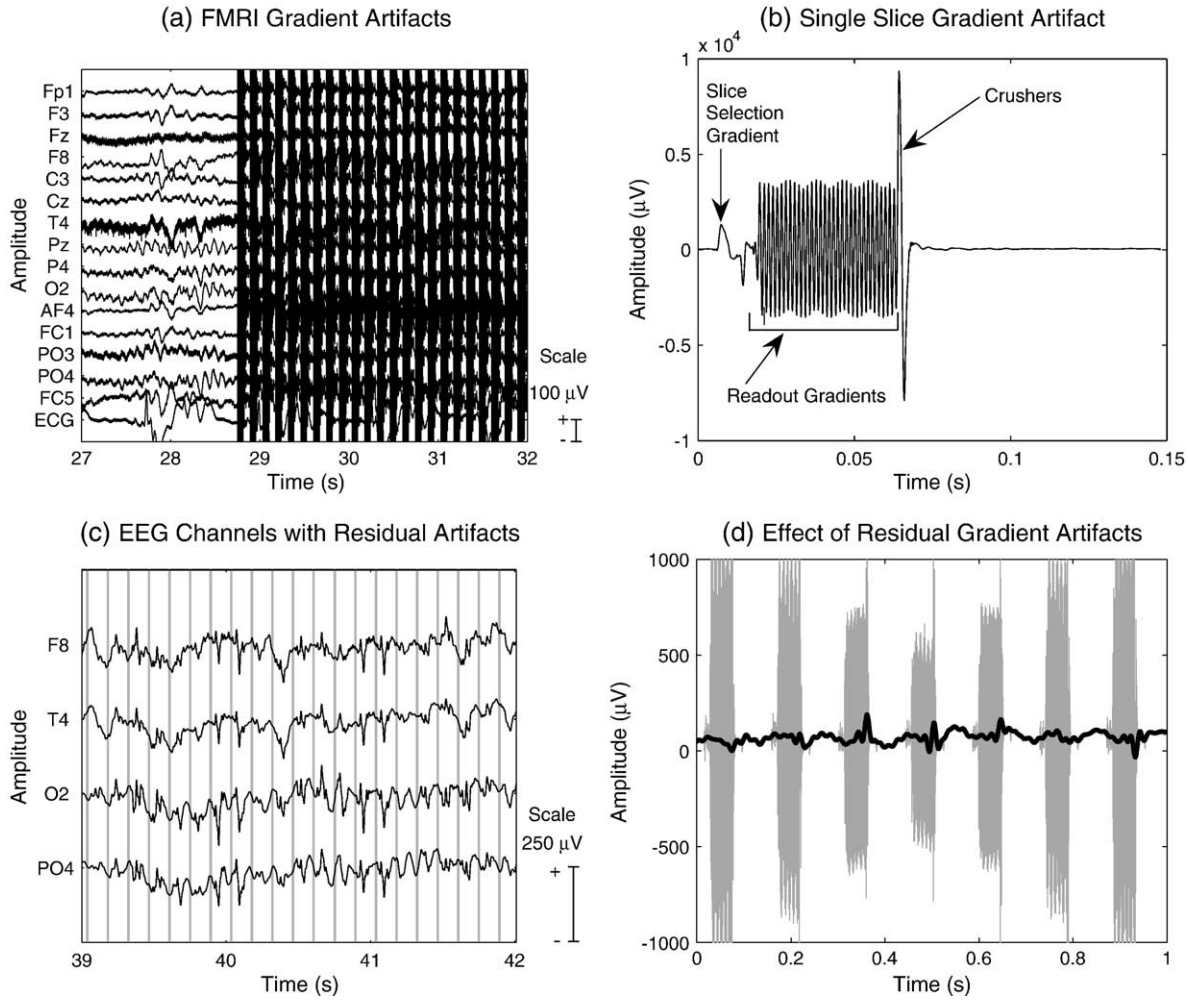

Fig. 1. Gradient artifact in EEG data. (a) The effect of FMRI on EEG data. Notice the high amplitude noise at approximately 29 s when scanning commenced. (b) The gradient artifact caused during the acquisition of a single slice in one of the EEG channels. Some features corresponding to the EPI sequence used are labeled. (c) Selected EEG channels with severe residual artifacts after cleaning with conventional average subtraction. The vertical grey lines indicate FMRI slice timings. The source of the residual imaging artifacts is the incomplete removal of the artifacts in the first place as shown in panel (d). The high amplitude signal shown in grey is the residual artifact before low-pass filtering. After low-pass filtering, these residuals are suppressed but still remain in the EEG-this is shown in black.

proposed (Bénar et al., 2003; Srivastava et al., 2005). One problem with these approaches is that they necessitate the presence of a large number of sensors. Also, the identification of artifact components can be subjective and is usually done manually. Most importantly, spatial filters assume that all the sensors are contaminated by common sources, which is not the case. The BCG artifact derives from sources that are rotating/moving, which contaminate different sensors at different points during the cardiac cycle with different effects. The most commonly used method for removing the BCG artifact is the average artifact subtraction (AAS) (Allen et al., 1998), in which a moving average artifact template is computed from successive artifact occurrences, then subtracted from the data. This assumes that the BCG artifact is a slowly changing signal that can be accurately captured by a moving average. This can result in residual artifacts in the data. A variation of this approach was used by Goldman et al. (2000), where instead of computing a simple moving average, a weighted average is used such that artifacts that lie further from the one being processed are less emphasized. Sijbers et al. (2000) and Ellingson et al. (2004) used a median filter to construct a template which is then scaled in time and amplitude to fit each artifact instance. Again, all these approaches assume a temporal relationship between the different occurrences of the artifact. Another central issue to such subtraction-based methods is the accurate detection of heartbeat locations. EEG systems often provide limited ECG recording facilities, e.g., one single bipolar channel. In addition, the ECG is usually distorted inside the MR machine due to blood conductivity (Wendt et al., 1988). These factors can lead to inaccurate detection of QRS peaks in the ECG, especially when simple thresholding detection methods are used (Allen et al., 1998).

Similar to the removal of the residual gradient artifacts, we propose a method where a basis set is constructed by performing temporal PCA on each EEG channel data. The basis set is then fitted to, and subtracted from, each artifact occurrence. This approach has the advantage of not assuming any temporal relation between the different occurrences of the BCG artifact in a given EEG channel. Rather, the assumption is that over a sufficient period of EEG recording from any single EEG channel, the different BCG artifact occurrences in that channel are all sampled from a constant pool of possible shapes, amplitudes and scales. The principal components

of all the occurrences can then describe most of the variations of the BCG artifact in that channel. This method is shown to be superior to AAS (Allen et al., 1998). In addition, an accurate, robust procedure based on the work of Christov (2004) followed by a correction algorithm is proposed for the accurate detection of QRS complexes in ECG data collected inside the magnet. The work of Negishi et al. (2004) also sheds some light on the usability of temporal PCA to remove BCG artifacts. However, they affirm that their results were somewhat unsatisfactory and more work was needed. More discussion about this is given later.

Methods

Gradient artifact removal

Our developed algorithm (FMRI artifact slice template removal, FASTR) is based on constructing a unique template for each artifact segment, in each channel, generated during the acquisition of a single FMRI slice. The algorithm comprises four stages. First, the signal is interpolated (up-sampled) and the slice-timing triggers are adjusted to optimize the alignment. Second, we perform a local artifact template subtraction, in which a moving average artifact template is constructed for each slice artifact then subtracted. Third, the artifact residuals are estimated using basis functions derived from performing PCA on each channel's artifact segments. The reason for splitting the artifact subtraction into two stages is that we need the algorithm to be as adaptive as possible; the algorithm needs to adjust to sudden changes in the artifact shape (due to head movement for example). Performing PCA repeatedly on small sections of the data (to make it adaptive) would produce less than optimal basis functions. On the contrary, the moving average subtraction performed in stage 2 is adaptive and removes more than 98% of the artifacts. Hence, we opted to make the bulk of the artifact removal as adaptive as possible while maintaining the efficiency of using PCA to describe and remove the residuals. Fourth, we perform adaptive noise cancellation (ANC) (Allen et al., 2000). ANC removes any components in the data that are correlated with a reference. By using the subtracted noise as a reference, artifact components not captured in the basis set are removed. More details about the function of the ANC filter is given later. The process encompassing all the four stages is referred to as FASTR. Fig. 2 shows a schematic of the FASTR algorithm. The schematic and the following details are for a single channel of EEG data.

Stage 1: slice-timing trigger alignment

During the acquisition of simultaneous EEG/FMRI data, triggers are sent by the MRI machine at the start of each slice acquisition. These triggers are usually a simple 5-V TTL signal that can be read by the EEG amplifier and inserted in the data to indicate the starting location of each slice acquisition and the corresponding slice artifact (to be used in subsequent steps to form the artifact template). However, since the MRI machine and the EEG system are driven by separate clocks, some degree of misalignment—"jitter"—may occur in the exact location of the registered trigger relative to the artefact from one slice to the next. The jitter gets worse as the EEG sampling rate is reduced. Relying on these triggers for time-locking slices to construct an artifact template would therefore not be optimal. To remedy this problem, the first channel data (or any other EEG channel data) is sinc interpolated (up-sampled) to bring the sampling rate to about 20 kHz and then divided into segments according to the slice-timing triggers. In this paper, the term artifact segment is used to indicate a window covering the duration of a single slice artifact occurrence. The first artifact segment is then taken as a reference. For each of the remaining slice artifact segments, the trigger location is adjusted to maximize the correlation with the reference. Although this process can be repeated for each EEG channel, this is not only computationally inefficient but is also unnecessary. We have found that in practice adjustments to one EEG channel apply equally to them all.

Stage 2: local slice artifact template subtraction

For any interpolated channel, $\mathbf{Y}^a$, which is collected during the acquisition of continuous FMRI, we also generate a 1-Hz high-pass filtered version, $\mathbf{Y}^h$. The high-pass filter serves to remove any slow drifts in the EEG to ensure that the different artifact segments used in the average artifact estimation have the same baseline. This is useful since the artifact signal itself is unlikely to have any slow drifts or shifts in the baseline from one segment to another, thus the high-pass filtering will improve the artifact estimation. $\mathbf{Y}^h$ is then segmented into N (N = volumes × slices) equal-sized segments according to the adjusted/aligned slice-timing triggers. Each of these segments is a $1 \times q$ vector, where q is the number of time points spanning each artifact interval. We then calculate the local moving average artifact template for each segment as:

$$\mathbf{A}_j = \frac{1}{|I(j)|} \sum_{\ell \in I(j)} \mathbf{Y}^h_\ell \tag{1}$$

In Eq. (1), $j = 1, 2 \ldots N$ indexes the slice artifact segments, $\mathbf{A}_j$ is a $1 \times q$ vector of the local moving average artifact template for segment j and ℓ is an index of the different artifact segments to be averaged. $I(j)$ is an index function, which determines which segments are included in the average. The slice segments in $I(j)$ are centered around segment j and are chosen so that there a is sufficient time gap between them to ensure that there is no EEG autocorrelation between the segments included in the template computation. This approach removes any data that correlates with the FMRI slice acquisition indiscriminately. The user needs only to determine how many elements to include in $I(j)$, i.e., the length of the moving average window, and how much gap to leave between the selected segments. The selection of averaging window length $|I(j)|$ governs the adaptivity of the algorithm to changes in the artifact waveform (due to head movement for example). The shorter the window length, the more adaptive the algorithm. On the other hand, the shorter the window length, the more noisy the artifact template and the more real EEG data are likely to be removed. The gap between selected segments should be judged by how close the segments are in time. Based on our experience, it is safe to assume that on the time scale of a slice artifact, EEG is uncorrelated after 350 ms. Hence, a gap of at least that much time should be left between successive segments included in the average. Finally, the computed template, $\mathbf{A}_j$, is scaled by a constant α to minimize the least squares between the template and the data. We can then subtract the scaled artifact from $\mathbf{Y}^h$ to construct a signal, $\mathbf{Y}^r$, which is the cleaned EEG data with residual artifacts.

Stage 3: gradient residual artifacts removal using optimal basis sets (OBS)

The vector $\mathbf{Y}^r$ that results from the previous step is still likely to be contaminated with residual artifacts due to slight variations in the shape of the artifact from one slice to the next. The amount of

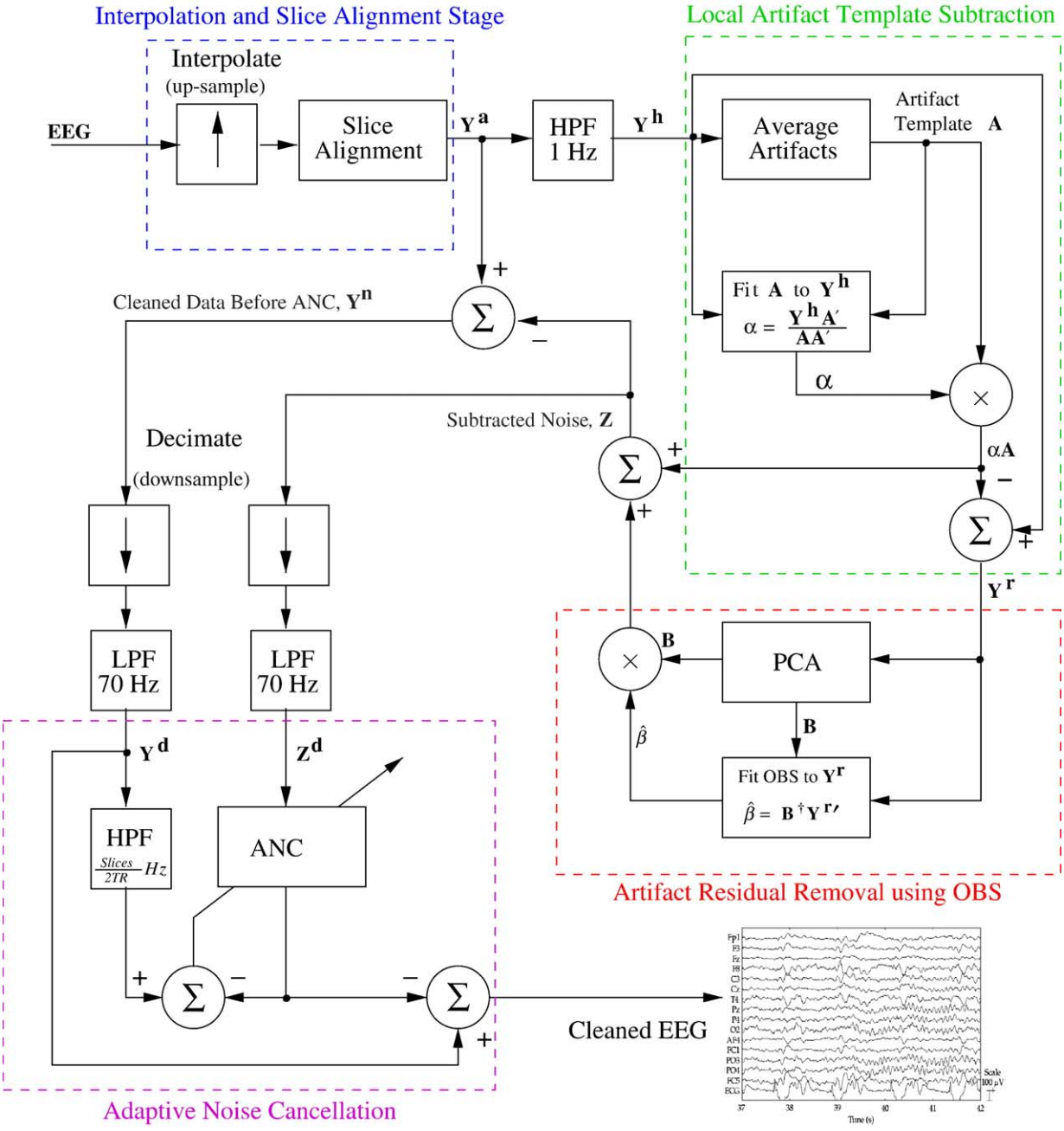

Fig. 2. Schematic flow chart of the FASTR algorithm. For each EEG channel, the signal is sinc-interpolated (up-sampled) and the slice-timing triggers are adjusted. The interpolated signal, $\mathbf{Y}^a$, is then high-pass filtered at 1 Hz to form a signal, $\mathbf{Y}^h$, which is then used to construct an average artifact template $\mathbf{A}$ for each slice segment. A scalar α is found from $\mathbf{A}$ and $\mathbf{Y}^h$ to minimize the least squares between each artifact and its template. Subtracting $\alpha\mathbf{A}$ from $\mathbf{Y}^h$ produces a cleaned EEG with residual gradient artifacts, $\mathbf{Y}^r$. $\mathbf{Y}^r$ is then used to construct an optimal basis set (OBS), $\mathbf{B}$, describing the residuals variations. $\mathbf{B}$ is fitted to each segment and a final noise signal, $\mathbf{Z}$, is formed. A further cleaned signal is calculated as $\mathbf{Y}^n = \mathbf{Y}^a - \mathbf{Z}$. Both $\mathbf{Y}^n$ and $\mathbf{Z}$ are low-pass filtered and down-sampled to the original frequency to form $\mathbf{Y}^d$ and $\mathbf{Z}^d$, respectively. $\mathbf{Z}^d$ is then used as a reference in the adaptive noise cancellation filter. The input to the filter is a high-pass filtered version of $\mathbf{Y}^d$. The output of the filter is then subtracted from the original $\mathbf{Y}^d$ to result in the clean EEG data.

variation is a function of the sampling rate and the synchrony between the clocks of the MRI and EEG systems. From $\mathbf{Y}^r$, we derive a set of basis functions for the residuals. First, a residuals matrix $\mathbf{S}_{p \times q}$ is formed, where p is the number of artifact segments included. As in the previous step, not all segments are included in $\mathbf{S}$. Instead of a fixed gap between the selected segments, however, segments should be selected after applying a gap of s or $s + 1$ in a random order, where s is the minimum gap determined in the previous stage. This is to safeguard against only capturing variations that occur every $s + 1$ segments and to insure that all variations of the artifact residuals are sampled. For example, if it were determined in stage 2 that one slice artifact segment should be skipped (i.e., $s = 1$) when calculating the local artifact, then in selecting segments to include in $\mathbf{S}$, we would sometimes skip one segment (s) and other times skip two segments ($s + 1$), in no particular order (randomly). The rows of $\mathbf{S}$ are then demeaned, i.e.,

the mean of each segment is removed. The column-wise mean is also calculated and subtracted from the columns of **S**, i.e., the mean effect of the residuals is calculated and removed. PCA is then performed on **S**. The different variations in the residual artifacts will be captured in the principal components of **S**, ordered according to the variance explained by each component. For simplicity, we use the term principal component (PC) to refer to the projection of **S** onto the principal component coefficients. The first C PCs, including the calculated mean effect, constitute an optimal basis set (OBS), $\mathbf{B}_{q \times C}$ for describing the gradient artifact residuals variations. The number of components C is selected based on the amount of variance explained by the PCs. It was observed that for most channels in a single data set, the same number of components is needed to explain the variance of the artifact. It is recommended that C is chosen conservatively, since including unnecessary components may result in the loss of data.

Each segment of $\mathbf{Y}^r$ can now be written in terms of **B** as:

$$\mathbf{Y}_j^{r'} = \mathbf{B}\boldsymbol{\beta}_j + \varepsilon_j' \tag{2}$$

where $\boldsymbol{\beta}_j$ is a $C \times 1$ vector of weights to fit **B** to $\mathbf{Y}^r$ and ε_j is a an error term for the segment. The weights for each segment are then estimated by least squares and added to the artifact noise found in stage 2 to construct the final estimation of the gradient artifacts, **Z**, and an artifact-subtracted EEG data $\mathbf{Y}^n$ (see Fig. 2).

Note that the final estimated noise is subtracted from the original interpolated EEG data, not the high-pass filtered version used for the artifact estimation, since the removed baseline drifts or slow oscillations might be of interest to the user. Both **Z** and $\mathbf{Y}^n$ are low-pass filtered at 70 Hz then down-sampled back to the original sampling frequency to form $\mathbf{Z}^d$ and $\mathbf{Y}^d$, respectively. Although stages 2 and 3 contribute to the same desired outcome, the approach taken in each is complementary to the other. In general, the process as a whole should be adaptive and accurate. Stage 2 works to remove the bulk of the artifact variance and is adaptive to sudden changes in the artifact shape. However, the moving average approach in stage 2 does not capture the exact artifact shape. Stage 3 serves to remove the details of the residuals. This necessitates that the OBS accurately describes the variations in the residuals. To this end, the residuals matrix **S** needs to have as many entries as possible for the PCA to produce an accurate OBS; this requirement limits the adaptivity of the OBS approach. At the same time, PCA need not be performed on the whole length of the recording. In our implementation, each 1-min portion of the data is processed at a time, partly for computer memory concerns, but also to provide a degree of adaptivity.

Stage 4: adaptive noise cancellation

As suggested by Allen et al. (2000), the final step is the removal of any remaining residuals using adaptive noise cancellation (ANC). Fig. 2 includes a schematic of the ANC filter. In ANC, a signal contaminated with noise constitutes the input to the filter, **Y**. The source of the noise is assumed to be known and is referred to as the reference signal. The actual noise in the signal is assumed to be correlated with the reference in an unknown manner. The ANC filter holds a vector of weights, which is used to calculate the output of the filter at each time point. The weights of the filter are updated at each time point using the least mean-square (LMS) algorithm. In general, the performance of the filter is controlled by the step size, μ, and the length of the weight vector, L, which control the stability and convergence of the filter. When the filter converges, it estimates the noise from the signal that is correlated with the reference. However, the accuracy of the estimation is limited by the quality of the reference and choice of μ and L. Also, high power fluctuations in the input can cause the filter to diverge. For in-depth examination of adaptive filters, see Haykin (1986).

In FASTR, the final artifact estimation $\mathbf{Z}^d$ is used as the reference in the ANC. In contrast, Allen et al. (2000) used a low-pass filtered, binary vector of 1s and 0s, where 1s indicates the slice timings as a reference in their implementation of ANC. Our choice of μ and L were similar to that of Allen et al. (2000); however, we have not investigated the optimization of these parameters in this work. Since ANC removes from the data components that are correlated with the reference, we think that the subtracted noise **Z** provides a more accurate reference for this purpose and was found to have less of an effect on real data. Additionally, the input to the ANC filter is a high-pass filtered version $\mathbf{Y}^d$. The cut-off frequency is selected to be half of the fundamental gradient artifact frequency, i.e., f_c = slices/2TR. The output of the filter is then subtracted from the original $\mathbf{Y}^d$ to produce the final clean EEG data.

We have found that the ANC filter consistently converged and removed components which were clearly related to the artifact. However, on its own it fails to adapt quickly enough to adequately remove all residuals. This is probably due to not providing an accurate enough reference. In addition, on its own, ANC occasionally diverges when applied to channels with high amplitude residuals. However, we have found that applying it as a last step removes any remaining residuals even though in most cases they are not detectable by visual inspection. These residuals can be due to the fact that the basis functions in the OBS do not perfectly describe all residual variations.

Heart beat detection

As a prerequisite to removing BCG artifacts, a robust QRS complex detection algorithm is needed. We propose a modification to the algorithm by Christov (2004) for the detection of the QRS peaks. In addition, we present a correction algorithm that operates on the results of the detection process to adjust for any false detection.

Combined adaptive thresholding

In the original algorithm, a *complex lead* is first constructed from several ECG channels. The algorithm is then applied to the complex lead. The signal constructed on which to apply the algorithm is referred to as the *complex lead*. As in most simultaneous EEG/FMRI experiments reported in the literature, ECG is recorded from a single bipolar channel and thus an alternative complex lead is needed. First, the ECG channel is band-pass filtered from 7 to 40 Hz. A moving average filter of samples in 28 ms intervals is then applied to suppress electromyogram noise (Christov, 2004). The complex lead is then calculated by applying the k-Teager energy operator (k-TEO) (Mukhopadhyay and Ray, 1998; Kim et al., 2004) to the filtered ECG, then setting all negative values to zero:

$$\mathbf{X}(n) = \max\left(\mathbf{E}^2(n) - \mathbf{E}(n-k)\mathbf{E}(n+k), 0\right) \tag{3}$$

where **X** is the complex lead, n is the time index, **E** is the filtered ECG and k is a frequency selection parameter (Kim et al., 2004).

By adjusting k, the TEO can be made sensitive to emphasize a desired frequency:

$$k = \frac{f_s}{4f_d} \tag{4}$$

where f_s is the sampling frequency and f_d is the desired frequency to emphasize. f_d is set to the 10th harmonic frequency of the ECG (usually around 10 Hz). Next, the combined adaptive thresholding algorithm is applied (Christov, 2004). An adaptive threshold (*MFR*) is applied to the complex lead **X**. The *MFR* threshold is calculated as the sum of three thresholds, *M*, *F* and *R*. A QRS peak is detected when $\mathbf{X}(n) \geq MFR(n)$. The reader is referred to the original paper (Christov, 2004) for a detailed discussion of the original algorithm, the different thresholds and their interpretation.

QRS peak correction algorithm

A binary vector of ones and zeros indicating peak locations, **P**, is created from the previous step, where a value of 1 indicates a QRS peak. The median, $\tilde{X}_{\mathrm{RR}}$, and standard deviation, σ_{RR}, of all RR intervals are calculated. **P** is divided into U 20-s sections, $\mathbf{P}_u^s$, where $u = 1, 2 \ldots U$. The different $\mathbf{P}_u^s$ sections overlap by 5 s. For any given $\mathbf{P}_u^s$ with Q peaks, i.e., Q ones in the section, there will be $Q - 1$ RR intervals. The RR intervals in each section are then calculated. For any $\mathrm{RR}(r) < (\tilde{X}_{\mathrm{RR}} - 3\sigma_{\mathrm{RR}})$, $\mathbf{P}_u^s\,(n_{\mathrm{RR}(r)})$ is set to zero, where $r = 1, 2 \ldots Q - 1$ is an index of the different peaks (ones) in each section and $n_{\mathrm{RR}}(r)$ is the time index n in $\mathbf{P}_u^s$ where $\mathrm{RR}(r)$ occurs. This implies that wherever the difference between two consecutive peaks is less than the median RR minus 3 times the standard deviation of all RR intervals, the second peak location is set to zero, i.e., the peak is removed. This process removes false positives. After all false positives are corrected for a section $\mathbf{P}_u^s$, the original **P** is updated before the next section is processed. The original ECG is then divided into equal segments according to the corrected peaks in **P** and the segments are averaged to form an average ECG beat waveform. This waveform is then taken as a reference and the peaks in **P** are adjusted as to maximize the correlation between each heart beat waveform in the ECG and the reference waveform. **P** is then divided again into U 20-s sections, $\mathbf{P}_u^s$, as described above and the RR intervals are calculated along with median RR for each section, $\tilde{X}_{\mathrm{RR}u}$. For any $\mathrm{RR}(r) > (1.5 \times \tilde{X}_{\mathrm{RR}u})$, $\mathbf{P}_u^s\,(n_{\mathrm{RR}(r-1)} + \tilde{X}_{\mathrm{RR}u})$ is set to 1. This means that wherever the difference between two consecutive peaks is more than 1.5 times the median RR for that section, a peak is added at time $\tilde{X}_{\mathrm{RR}u}$ after the first peak, i.e., a peak is added where missing. This process corrects for false negatives. After all false negatives are corrected for a section $\mathbf{P}_u^s$, the original **P** is updated before the next section is processed. Finally, the peaks in **P** are again adjusted using correlation as described previously.

Ballistocardiographic artifact removal

Like gradient artifact residuals, BCG artifacts are time varying. However, the variations in BCG artifacts are unpredictable and more difficult to characterize. We assume that each occurrence of a BCG artifact, in any given EEG channel, is independent of any previous occurrence. Moreover, we assume that the different occurrences are sampled from an unknown set of possible variations. These assumptions present the use of OBS as an ideal solution, where the principal variations can be captured by doing a PCA analysis on a matrix of BCG artifact occurrences. First, all QRS peaks are shifted forward in time by 210 ms, which is a standard delay between QRS complexes and the occurrence of BCG artifacts (Allen et al., 1998). Then, for each channel in the EEG data, all BCG artifact occurrences are aligned in a matrix and PCA is performed. The first 3 PCs (including the mean effect) are taken as an OBS. The OBS is then fitted to, and subtracted from, each BCG artifact occurrence. The process is repeated for each channel.

Implementation

All algorithms were implemented in Matlab® (The MathWorks, Inc., MA, USA) as plug-ins for the EEGLAB Toolbox (Delorme and Makeig, 2004) and they can be downloaded for use under the General Public Licence (GPL-Free Software Foundation, Inc., Boston, MA). EEGLAB was also used in the validation and visualization of the methods including most of the EEG time series and topographical plots.

Validation

Data acquisition equipment

EEG and ECG data were recorded using the SystemPLUS EEG system and an SD32 MRI amplifier (Micromed s.r.l., TV, Italy). The system is capable of recording from 30 common reference EEG channels and two bipolar channels to be used for electromyogram (EMG), electrocardiograph (ECG) or electrooculogram (EOG) recordings. All channels had 10 kΩ current limiting resistors and 600 Hz, 20 dB/decade low-pass filters to protect against RF noise. All channels also had 0.15 Hz, 40 dB/decade high-pass filters. A SigmaDelta analog-to-digital converter (ADC) with anti aliasing filtering was used. The system had a sampling frequency of 2048 Hz, a dynamic range of ±25.6 mV and a resolution of 12.2 nV. The headbox containing the amplifiers, filters and ADC hardware is placed in the scanner room and the signal is transmitted via optical fibers to the acquisition workstation in the console room. FMRI was performed using a 3-T Varian Inova scanner. Excitation (slice-timing) triggers from the MRI machine were recorded in the EEG data.

Gradient artifact removal

EEG data were collected during continuous FMRI using an echo planar imaging (EPI) sequence. For the purpose of this validation, EEG was collected from only 15 EEG channels: FP1, F3, Fz, F8, C3, Cz, T4, Pz, P4, O2, AF4, FC1, PO3, PO4 and FC5 according to the 10–20 international system. All channels were referenced to a common electrode at the FCz location. The ECG was recorded using a single bipolar channel. 40 FMRI volumes were collected with a TR = 3 s and 21 axial slices per volume for a total scanning time of 2 min. The subject was instructed to open and close his eyes in periods of 10 s during scanning using the scanner communication system and earphones. EEG was also recorded while the subject repeated the same task inside the scanner but without FMRI.

The data were first cleaned using just the subtraction of the local average artifact template, then channels with visible residual gradient artifacts were used for validation comparisons. The following EEG channels had visible residual gradient artifacts and were used in the validation: F8,T4, Pz, P4, O2 and PO4. We refer to these channels as the *validation channels*.

FMRI artifact frequencies overlapping the EEG frequency band occur in discrete frequency intervals—"bins". The fundamental frequency bin is the number of slices collected per second, e.g., for 21 slices collected during a TR of 3 s, the artifact frequency bins will be 7, 14, 21 Hz … etc. Leakage into the ±1-Hz region around these bins is observed. To assess the performance of each stage of the algorithm, the power in the 7-, 14-, 21-, 28- and 35-Hz frequency bins is compared before and after the slice alignment and the PCA/OBS steps. Frequencies above 35 Hz can be removed using low-pass filtering since they are generally not of biological interest. The same comparison is also performed between the complete FASTR and IAR algorithms (Allen et al., 2000). The implementation of IAR used did not incorporate the interpolation scheme described by Allen et al. (2000), as this requires the availability of a high-resolution slice-timing signal, which was not available in this study. Allen et al. (2000) used a slice-timing signal with a resolution of 10 μs as a reference to interpolate the artifact segments before calculating the average artifact template. This will inevitably render the performance of the implemented IAR algorithm suboptimal, resulting in severe residual artifacts. However, this test is not aimed at evaluating the general performance of IAR, but rather to compare its performance to FASTR given a generic setup with limited capabilities, i.e., low sampling frequency for both data and slice-timing signal. In addition, assuming that the performance of FASTR would resemble that of IAR after the slice-trigger alignment and average artifact removal steps, ANC was applied after these two steps to demonstrate its inability to totally remove the residuals on its own. No explicit comparison was done with raw, uncleaned data since the effectiveness of the average artifact subtraction principle has already been thoroughly demonstrated (Allen et al., 2000; Salek-Haddadi et al., 2003; Bénar et al., 2003). The aim here is to demonstrate the effectiveness of the slice alignment and PCA/OBS for reducing the residuals and compare the overall performance with the results achieved using the IAR method (Allen et al., 2000), given the available setup and hardware.

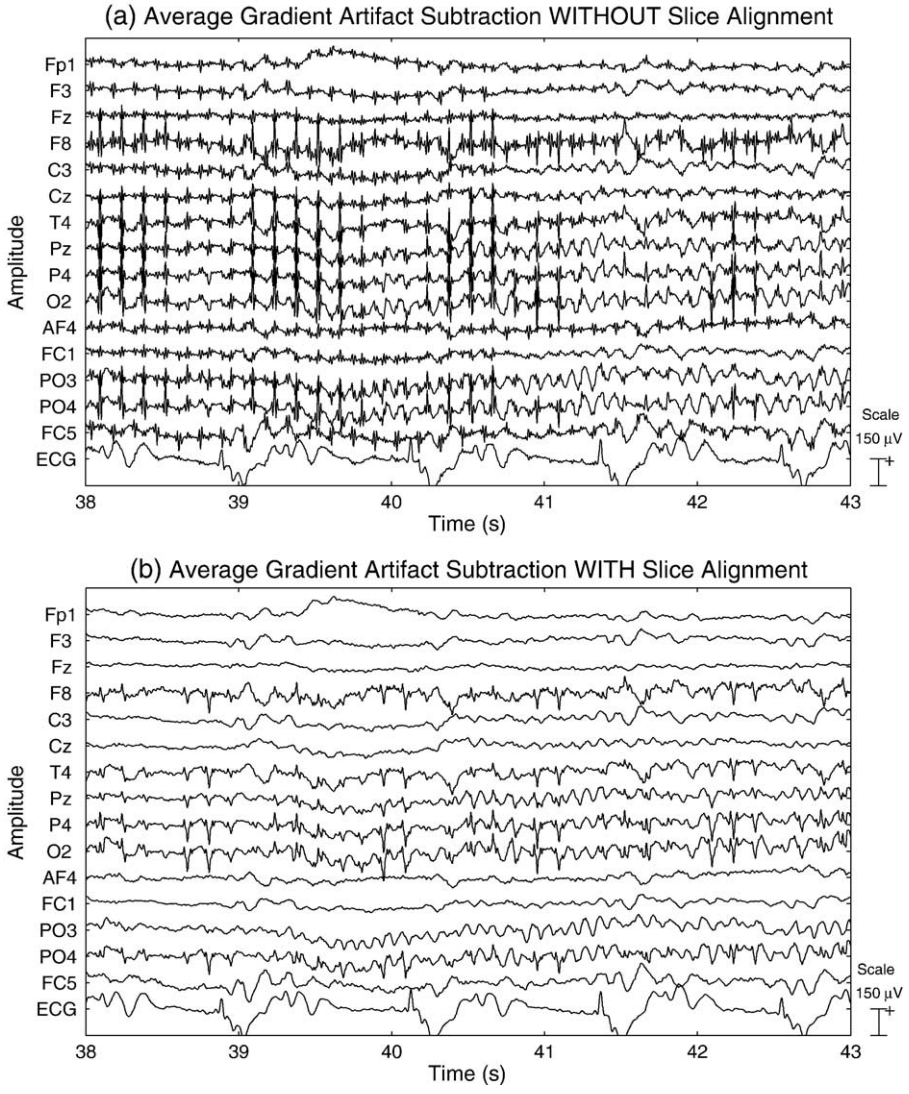

Fig. 3. Quality of EEG after cleaning gradient artifact using only local artifact template subtraction without slice alignment (a) and with slice alignment (b). It is clear that slice-timing triggers alignment has a profound effect on the quality of the cleaned data especially for data collected at low sampling rates.

Qualitatively, the EEG was examined for features known to be in the data. One kind of feature is the BCG artifacts. Such artifacts are recorded even without scanning and have distinct, repetitive shape for each channel. The EEG was examined to see if these signals are still present after the FASTR algorithm. The other feature is the alpha rhythm (~10 Hz), which appears on posterior electrodes when the eyes are closed. The appearance and disappearance of the alpha rhythm according to the experimental task was examined and the data were compared to that collected without FMRI, while performing the same task. Finally, the quality of the cleaned ECG signal was also examined. Unlike the EEG, the ECG has a unique shape and features, and any distortion or loss of data can be easily noticed.

Heart beat detection

The ECG of 10 subjects was collected during FMRI and processed to remove the gradient artifacts. The quality of each ECG data was subjectively classified as poor, good or excellent depending on the visibility of the QRS complex and its peak height relative to other features in the signal such as the T wave. For each ECG recording, the total number of QRS complexes/heart beats was counted manually. This total count is considered the true positive number, T_P, of QRS complexes. Any QRS complex not detected by the algorithm was considered a false negative, F_N. Any QRS complex detected in the absence of an actual QRS complex was considered a false positive, F_P. If a QRS complex was detected but its position had a time-shift error, i.e., the algorithm indicated the location of the QRS a little early or late, this was considered both as a false negative and a false positive. The sensitivity, S_e, and specificity, S_p, were then calculated for each data set as:

$$S_e = \frac{T_P}{T_P + F_N} \tag{5}$$

$$S_p = \frac{T_P}{T_P + F_P} \tag{6}$$

Ballistocardiographic artifact removal

Eight data sets from subjects participating in a simultaneous EEG/FMRI experiment (see the companion paper by Iannetti et al., this issue) were used. The data were 23 min in duration and were cleaned of gradient artifacts using the FASTR algorithm.

Two quantitative tests were used. For the first test, each data set was divided into epochs each spanning −0.5 to 1.2 s around a QRS peak. The average BCG artifact was then found for each channel by averaging all epochs. Assuming no correlation between the EEG and the QRS peaks, this produces the average BCG artifact for each channel in each data set. The mean power of the BCG artifact in each channel was then calculated by taking the mean of the squares of each average BCG artifact. The same procedure was applied to the same data sets after removing the BCG artifacts using the OBS and AAS (Allen et al., 1998) methods to estimate the residual BCG artifact. The amount of residual BCG artifact power (in % of original power) in each channel was compared for both methods. The results were averaged over all data sets. The limitation of this test is that it

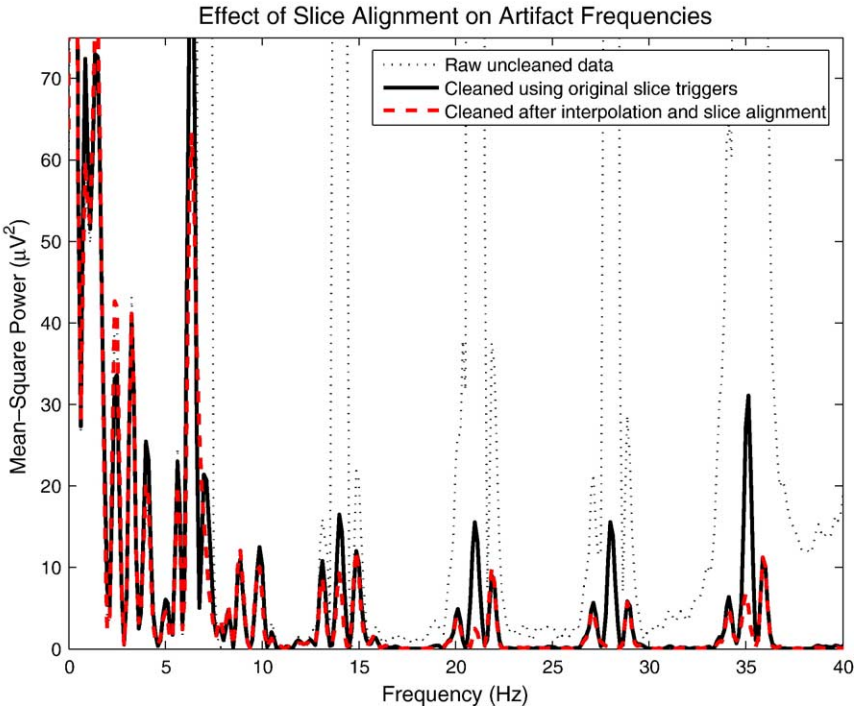

Fig. 4. Effect of slice-timing triggers alignment on the power of gradient artifact frequencies. The black dotted trace shows the power spectrum of a typical EEG channel before cleaning any artifacts. The fundamental frequency bins of the artifact can clearly be seen at 7, 14, 21, 28 and 35 Hz. The solid black line is the same channel after removing the local average artifacts without slice alignment, i.e., stage 2 only of FASTR. The dashed red line is the same channel cleaned after interpolation and slice alignment, i.e., stages 1 and 2 of FASTR. The reduction in power at the artifact fundamental and harmonic frequencies is apparent.

assumes that the residuals will not be random, and thus can be captured in the average, i.e., if the residuals left by the algorithm are not similar from one occurrence to another (i.e., random) they will cancel each other out and will not be detected in this test. On the other hand, this test has the advantage of not including any real EEG information in the estimate of the residuals, assuming the EEG is uncorrelated with the cardiac cycle and will cancel out in the average.

For the second test, a measurement of the artifact energy computed from the power spectrum was used. For each data set, the power spectrum of each channel data was computed. Also, the first ECG harmonic frequency was found from the ECG data. The BCG artifact has a power spectrum similar to the ECG, with power peaks at the harmonics of the heart rate. The energy of the BCG artifact in each channel was found by summing the power from the first ten harmonics. This measurement is repeated after removing the artifact using both the OBS and AAS (Allen et al., 1998) methods. Again, the results were averaged over all data sets. In this test, no assumption about the repetitiveness of the residuals is made. However, this test is limited by the fact that the harmonic frequencies of the BCG artifact will inevitably also contain information about the EEG signal.

Qualitatively, the algorithm was applied to data sets of subjects performing a paradigm involving opening and closing the eyes to examine the quality of the recovered alpha rhythm elicited by this procedure.

Application to laser-evoked potentials recorded during FMRI

The algorithms described in this paper have been applied to EEG data collected simultaneously with FMRI during laser nociceptive somatosensory stimulation. A companion paper describes in detail the feasibility of recording laser-evoked potentials (LEPs) during simultaneous FMRI and shows that LEPs collected during FMRI are not significantly different from LEPs collected in control

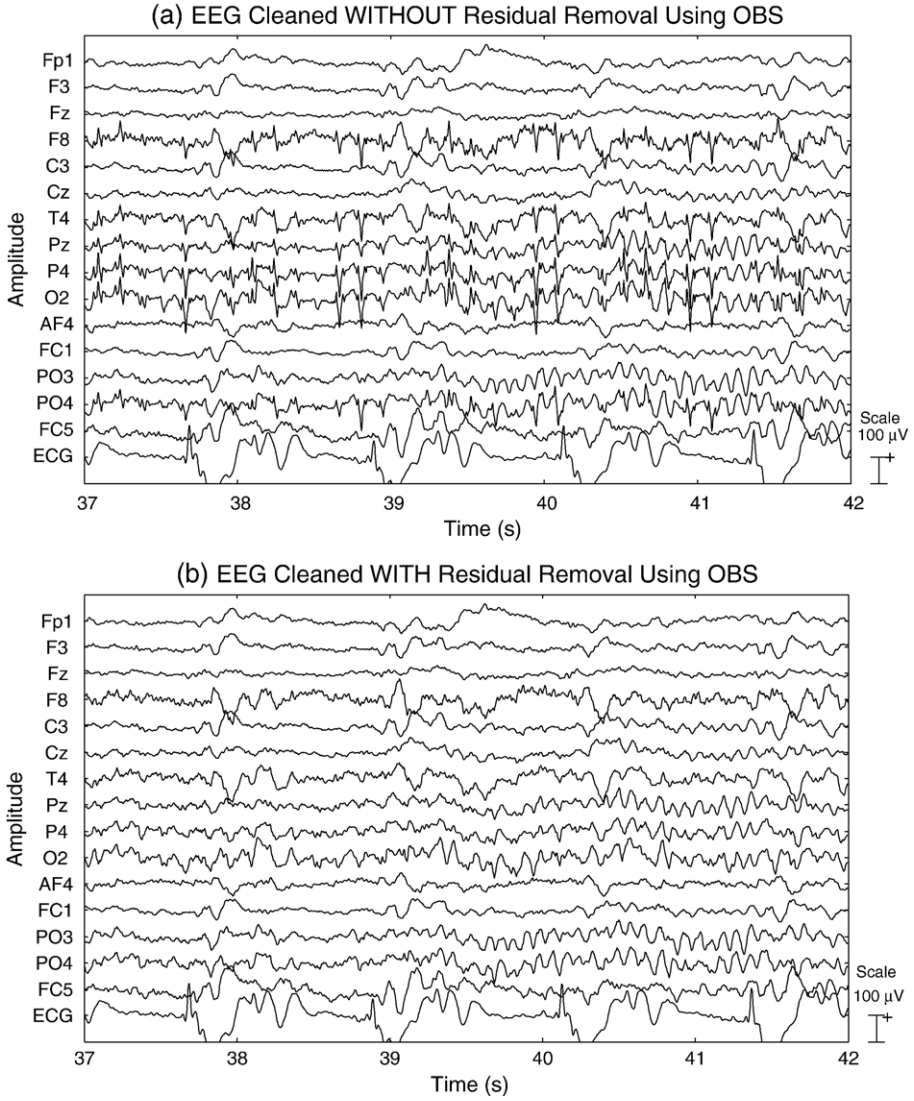

Fig. 5. Effect of residual estimation and removal using OBS on EEG data quality. (a) EEG traces after stages 1 and 2 of the FASTR algorithm, i.e., slice-timing triggers alignment and local moving average subtraction, but without residual estimation and removal using OBS. (b) The same trace after using OBS to remove the gradient artifact residuals.

sessions outside the scanner using the same equipment and experimental design (Iannetti et al., this issue).

Results and discussion

Gradient artifacts removal

In the first stage of the FASTR algorithm, the slice-timing triggers are adjusted to ensure that the moving average captures the best possible representation of the local artifact.

In Fig. 3 the effect of slice-timing trigger alignment on the quality of the cleaned EEG data can clearly be seen. Both plots in Fig. 3 are cleaned only by removing the local average slice artifact. The top plot shows EEG data cleaned using the original triggers recorded during imaging, i.e., performing stage 2 of the FASTR algorithm only. The bottom plot shows EEG data cleaned after interpolation and trigger alignment, i.e., cleaning using stages 1 and 2 of the FASTR algorithm. The severity of the residual artifacts due to not adjusting the position of the slice triggers is directly proportional to the sampling frequency of the EEG, as expected when asynchronous clocks drive the EEG and MRI systems. This is quite a common scenario given any independent MRI and EEG equipment not modified to be driven by a linked clock.

Fig. 4 shows the power spectrum of an EEG signal from a representative channel before any artifact removal and after the removal of the local average artifact with and without slice-timing trigger alignment. A significant reduction of power in the artifact frequency bins is found. On average in these channels, slice-timing trigger alignment reduced the power in the 7-, 14-, 21-, 28- and 35-Hz frequency bins by 8.5%, 16.2%, 36.7%, 48.5% and 45.8%, respectively.

Residuals after stages 1 and 2 of FASTR can still be seen in the validation channels. Fig. 5 shows the EEG before and after applying OBS fitting and subtraction to the residuals. It is clear that the remaining residuals have been removed from the six contaminated channels. The other channels do not exhibit any obvious changes in the quality.

Fig. 6 shows the power spectrum for a typical residual-contaminated EEG channel before and after OBS fitting and subtraction. Again, the power at the artifact frequency bins is greatly reduced. On average in the validation channels, the artifact powers were reduced at the 7-, 14-, 21-, 28- and 35-Hz frequency bins by 30.4%, 45.2%, 85.9%, 88.7% and 70.1%, respectively, compared to the previous stage.

The final stage in FASTR is adaptive noise cancellation. Fig. 7 demonstrates how ANC is unable to remove all residual artifacts on its own. ANC in Fig. 7 was applied to the output of FASTR after slice-timing trigger alignment and average artifact removal only, assuming that the output of this would resemble IAR if an interpolation scheme was possible using a high resolution slice-timing signal.

It was noticed that using the subtracted overall noise from stages 1 to 3 as a reference in the filter instead of a binary vector was less likely to remove real data. This was noticed in the shape of the BCG artifacts, since they appeared to be slightly distorted from their original shape after ANC using a binary reference, whereas using the subtracted noise as a reference did not cause the shape to distort. Both, however, seemed to have similar effect on further removing any remaining residuals.

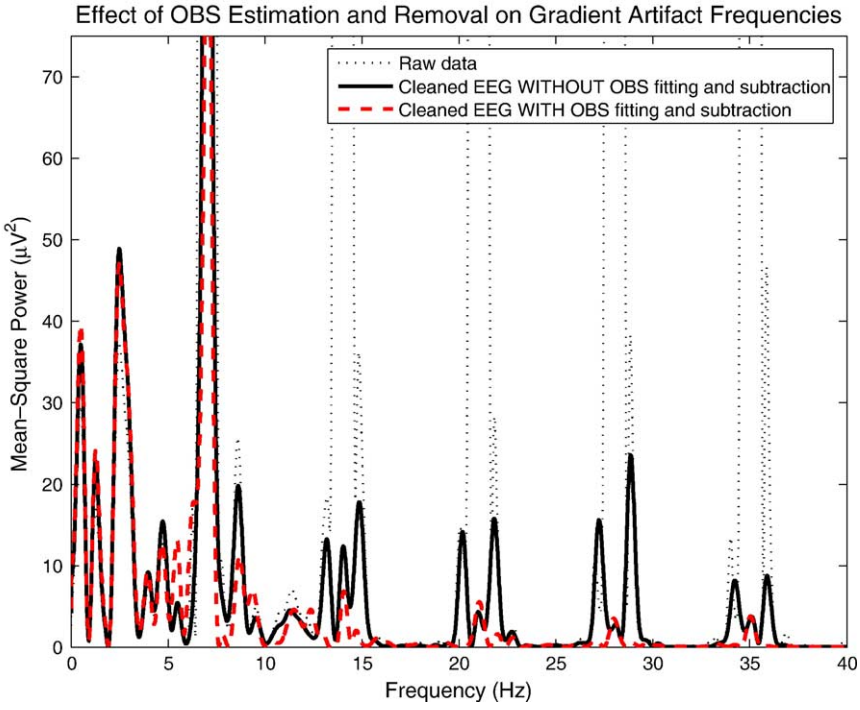

Fig. 6. Effect of OBS estimation and removal on the power of gradient artifact frequencies. The black dotted trace shows the power spectrum of a typical EEG channel before cleaning any artifacts. The fundamental frequency bins of the artifact can clearly be seen at 7, 14, 21, 28 and 35 Hz. The solid black line is the same channel after slice trigger alignment, removal of local moving average artifacts but without OBS estimation and removal, i.e., stages 1 and 2 only of FASTR. The dashed red line is the same channel cleaned after slice trigger alignment, removal of local moving average artifacts and OBS estimation and removal, i.e., stages 1 through 3 of FASTR. The reduction in power at the artifact fundamental and harmonic frequencies is clearly visible.

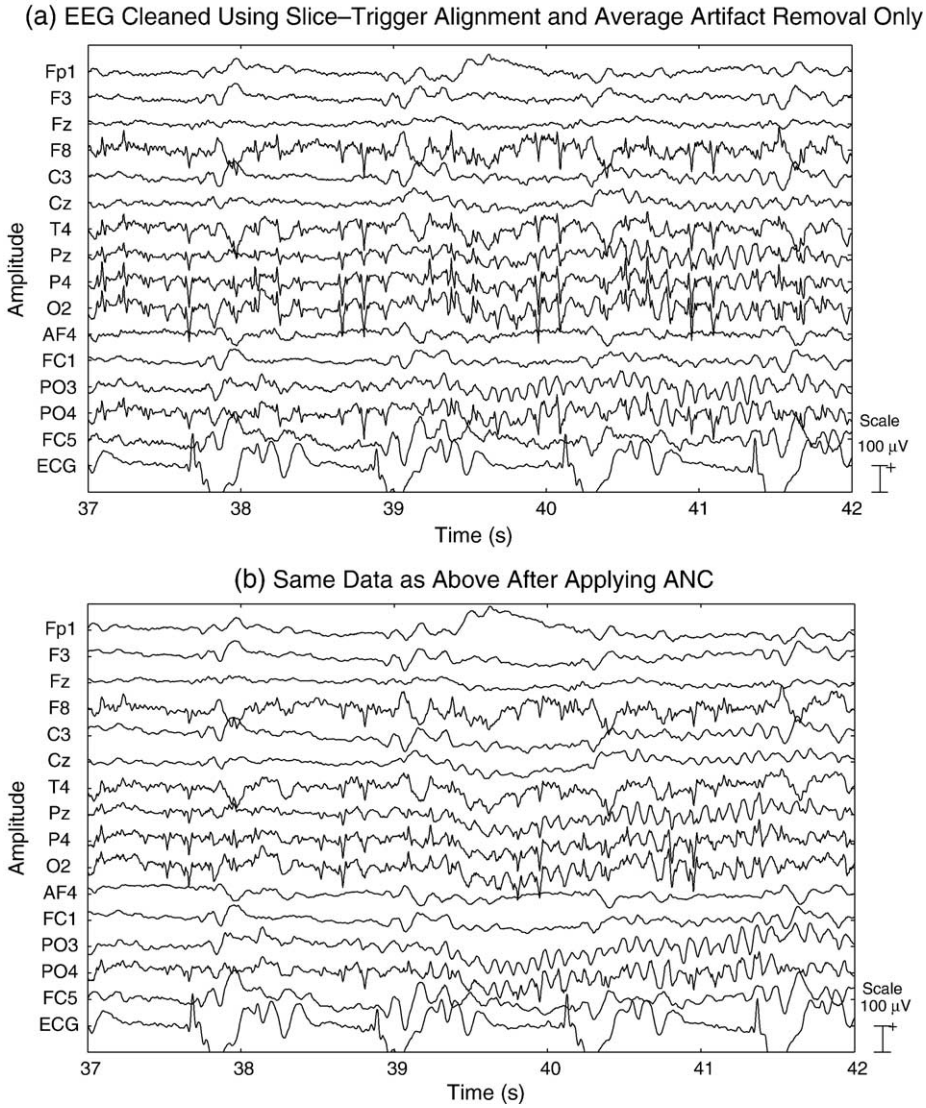

Fig. 7. Limited effectiveness of ANC for the removal of residual gradient artifacts. (a) EEG traces after stages 1 and 2 of the FASTR algorithm, i.e., slice-timing triggers alignment and local moving average subtraction, but without residual estimation and removal using OBS or ANC. (b) The same trace after using ANC only to remove the gradient artifact residuals. Although ANC reduces the residual artifacts by about 50%, it is unable to completely resolve the problem.

For the final validation of FASTR, the results of the whole FASTR algorithm (i.e., stages 1–4) were compared to the results of IAR plus ANC as proposed by Allen et al. (2000), excluding the interpolation scheme. Fig. 8 shows EEG data cleaned with FASTR and IAR and compares them to EEG data collected inside the scanner but without any scanning. Overall, using FASTR results in cleaner EEG with quality that rivals EEG collected without any scanning. Data collected during and without FMRI both had the same paradigm of opening and closing the eyes. In the section of data shown, the subject closed his eyes at approximately 39.5 s in the data collected during FMRI (a and b) and at approximately 10.5 s in the data collected without scanning. The eye closure events are aligned in the data sets and the alpha rhythm can clearly be seen in the posterior electrodes. Additionally, the BCG artifacts can also be seen correlated with the ECG; a feature known to exist in the data. The ECG is also shown to be preserved.

Fig. 9 shows the power spectrum for a typical residual-contaminated EEG channel before and after removing the gradient artifacts using both the IAR and FASTR algorithms. The power at the artifact frequency bins is greatly reduced when using FASTR compared to IAR. On average in the validation channels, the artifact powers were reduced at the 7-, 14-, 21-, 28- and 35-Hz frequency bins by 32.3%, 13.1%, 51.6%, 63.6% and 87.8%, respectively, when using FASTR compared to IAR.

Heart beat detection

Of the ten ECG recordings used, one was rated to be excellent, six were rated good, while three were judged to be of poor quality. A sample of different ECG signals is shown in Fig. 10. In recordings designated as poor, the QRS complexes were subtle, which would make the use of simple thresholding techniques to detect the peaks unreliable. The average sensitivity

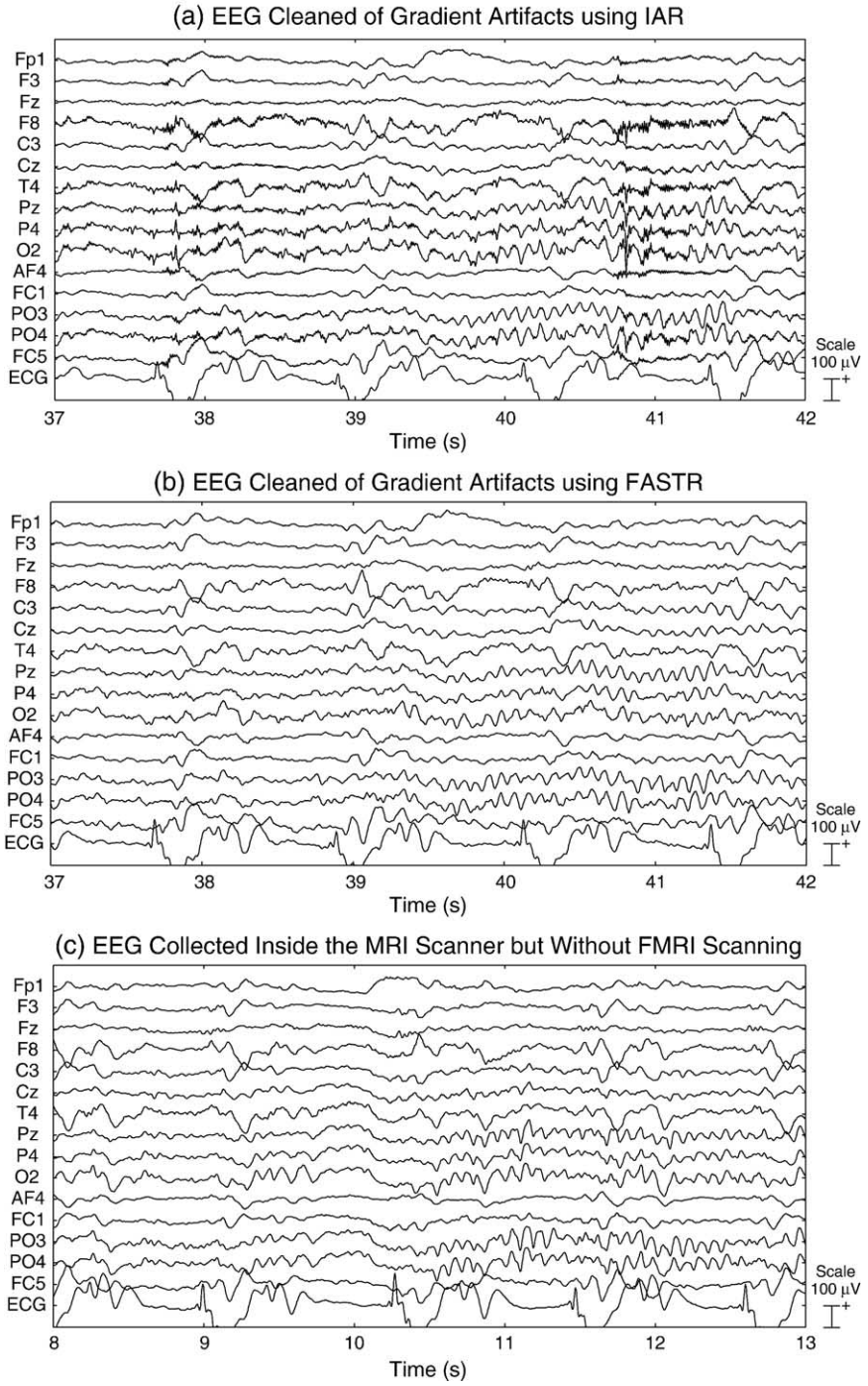

Fig. 8. Comparison of (a) the IAR algorithm (Allen et al., 2000), (b) FASTR algorithm and (c) data collected without FMRI. The superior quality of the FASTR algorithm can clearly be seen. The close resemblance between the data cleaned with FASTR and the data collected without FMRI can be observed. As the subject closed his eyes at 39.5 s for panels a and b, and at 10.5 s for panel c, the alpha rhythm appears in electrodes Pz, P4, O2, PO3 and PO4.

achieved by the algorithm was 99.27% (±0.9%) and the average specificity was 98.98% (±1.3%). In the worst case, the algorithm achieved a sensitivity of 97.35% and a specificity of 96.5%. In two data sets, the algorithm achieved 100% for both specificity and sensitivity. It is evident that the algorithm, combined with the correction procedure, is capable of detecting QRS events quite accurately even for ECG recordings of poor quality. This is a crucial result since subtraction-based methods for BCG artifact removal are dependent on the accurate detection of QRS events.

Ballistocardiographic artifact removal

A comparison between the performance of OBS and AAS (Allen et al., 1998) is shown in Figs. 11–13. Fig. 11 plots the amount of average BCG artifact residuals after cleaning the data

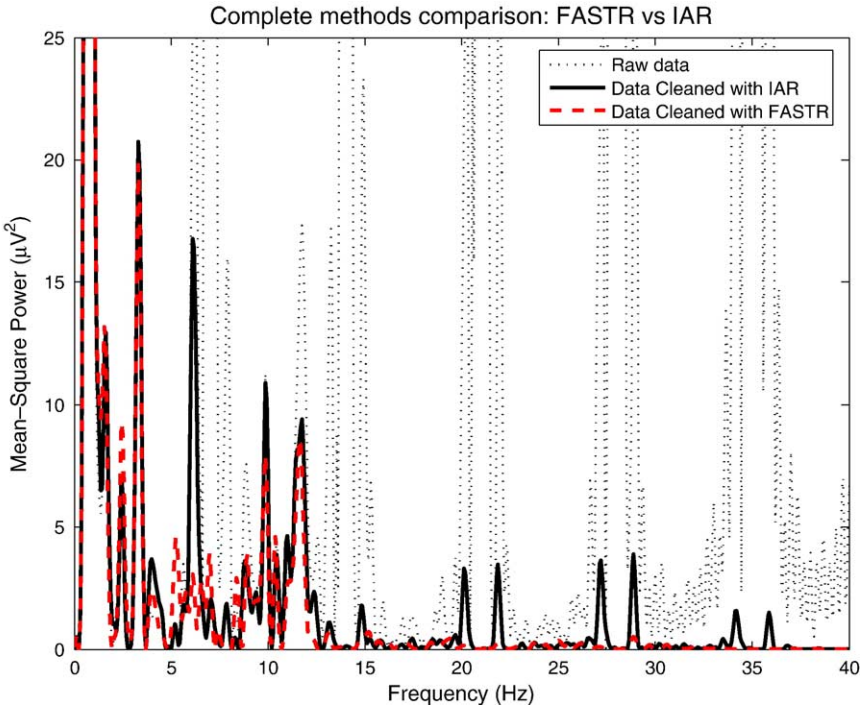

Fig. 9. Frequency spectrum comparison between EEG data cleaned of gradient artifacts using IAR (Allen et al., 2000) and the FASTR algorithm. The black dotted trace shows the power spectrum of a typical EEG channel before cleaning any artifacts. The artifact can clearly be seen at 7, 14, 21, 28 and 35 Hz. The solid black line is the same channel cleaned using the IAR algorithm plus adaptive noise cancellation using a binary reference. The dashed red line is the same channel cleaned using the complete FASTR algorithm.

with OBS and AAS. The height of each bar is the average percentage of the original BCG artifact power remaining in each channel. The results shown are the average over 8 data sets. On average, using OBS left 2.7% (±1.3%) residuals while AAS left 4.0% (±4%) ($P < 0.05$ using a two-tailed paired t test) of the original BCG artifact power. Fig. 12 compares the

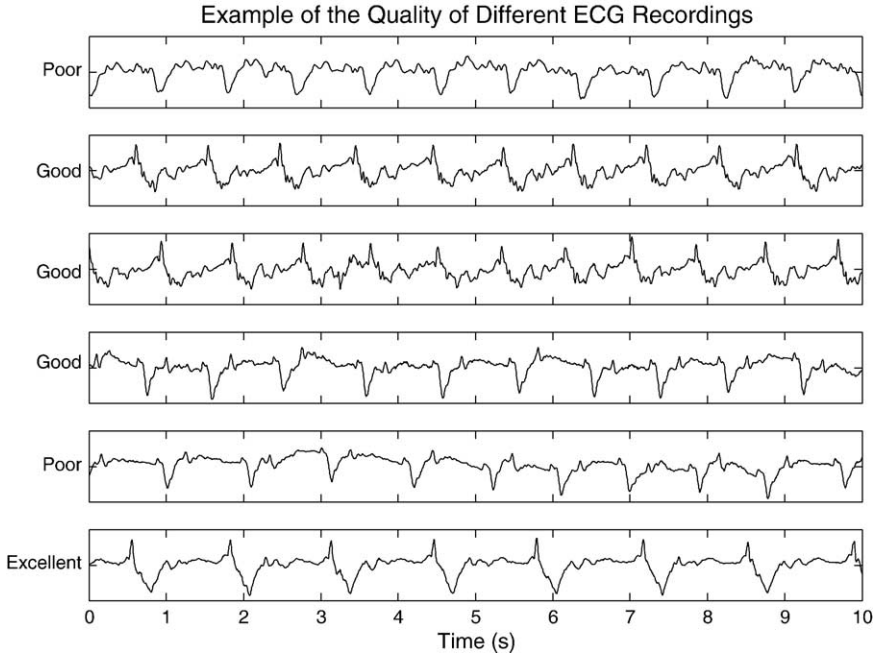

Fig. 10. ECG recordings of different quality. The subjective ratings of poor, good and excellent are given depending on how distinct the QRS complexes are in the signal and on their height compared to other parts of the signal. It can be seen that, for example, in poor signals the QRS is very subtle and the signal is dominated by the augmented T wave. On the other hand, in the excellent signal the QRS complexes are very visible, distinct and their peaks are higher than any other features in the signal.

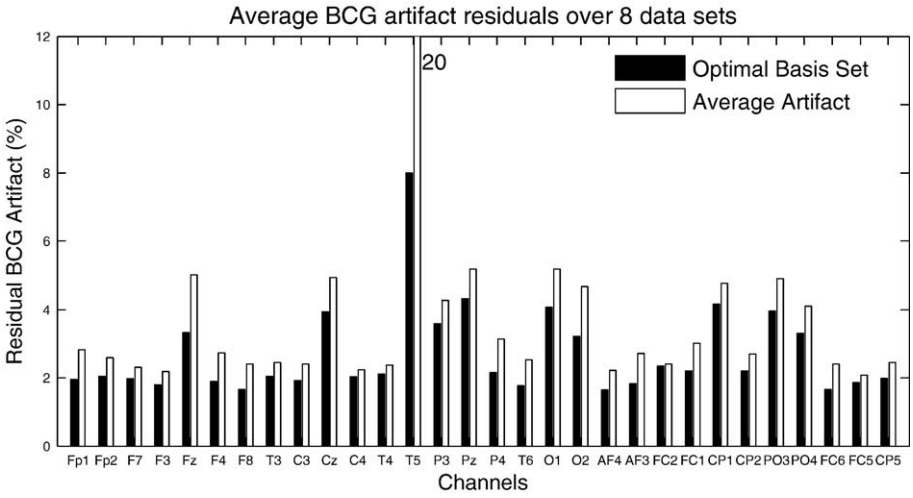

Fig. 11. Plot illustrating the amount of BCG artifact residuals left by the AAS and OBS methods. The height of each bar is the percentage of the original BCG artifact power for that channel that still remained as residuals after cleanup. The shown results are the average over 8 data sets. On average using OBS left 2.7% (±1.3%) residuals while AAS left behind 4.0% (±4%) of the original BCG artifact power.

BCG residual artifact energy computed from its power harmonics after removing the artifact using the AAS and OBS methods. The figure presents the data as percentage of the original BCG artifact energy and are the average over 8 data sets. On average, using OBS left 29% (±12%) of residual energy while AAS left behind 35% (±15%) ($P < 0.005$ using a two-tailed paired t test). Fig. 13 is a topographical plot comparing the residuals left by both methods from a typical data set. Again, it can be seen that the amplitude of the average BCG residual is greater in virtually all channels when using AAS compared to OBS.

Qualitatively, Fig. 14 shows EEG data before and after BCG artifact subtraction for an eyes open/eyes closed experiment. The preservation of the alpha rhythm can be seen in posterior EEG channels, i.e., Pz, P4, O2, PO3 and PO4, when they occur at about 4.5 s as the subject closed his eyes.

Discussion

Simultaneous EEG and FMRI is a potentially powerful technique in functional neuroimaging. Along with the potential benefits, comes a series of challenges in implementing such a technique. The main obstacles are artefacts from MRI gradients and ballistocardiographic effects, as well as the need for practical implementations of methods for their removal.

Removing gradient induced artifacts from simultaneously collected EEG data using subtraction-based methods has been shown to be effective before (Allen et al., 2000; Salek-Haddadi et al., 2003; Bénar et al., 2003). These methods offer the most practical solution as they do not require hardware modification such as to synchronize the EEG and MRI system or alter the imaging sequence (Anami et al., 2003). To date, however, these methods require data to be collected at very high sampling

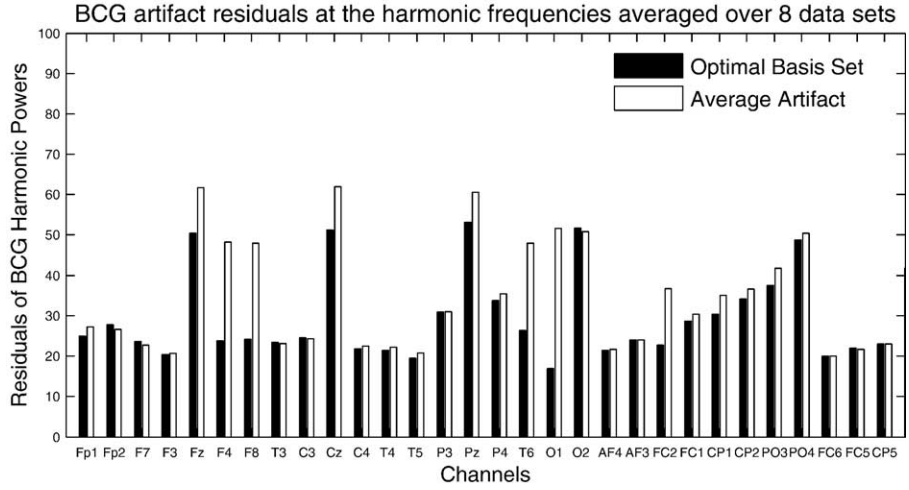

Fig. 12. Plot illustrating the amount of BCG artifact residuals left by the AAS and OBS methods at the harmonic frequencies of the artifact. The height of each bar is the percentage of the original BCG artifact power sum over the first 10 harmonics for that channel that still remained as residuals after cleanup. The shown results are the average over 8 data sets. On average using OBS left 29% (±12%) residuals while AAS left behind 35% (±15%) of the original BCG artifact power.

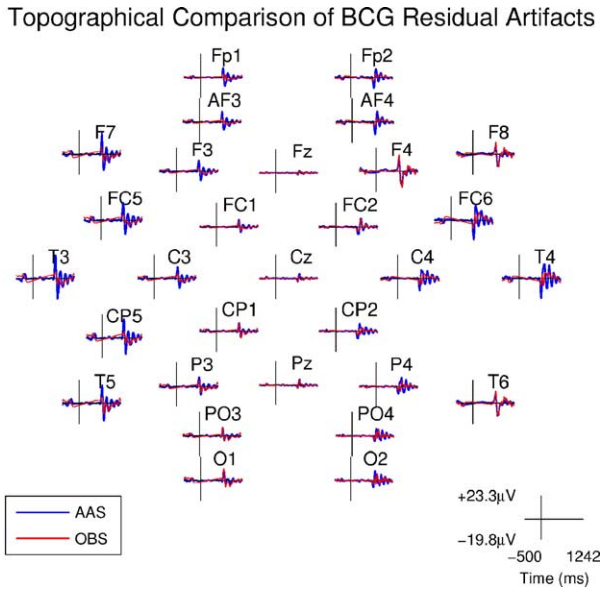

Fig. 13. A topographical plot showing the average BCG artifacts residuals in the EEG of a typical subject using both AAS and OBS methods. In comparison to the residuals left by AAS (blue), the residuals left by OBS (red) are clearly smaller in amplitude in most channels.

frequency in order to avoid serious residual artifacts. From our experience, some commercially available subtraction-based methods suffered from residuals even when the data were sampled at as high as 10 kHz. At such sampling frequencies, however, the practicality of running experiments is extremely limited as the data size fast becomes very large, limiting the duration of the experiment. We have developed an algorithm which removes gradient artifacts and any residuals from data sampled at only 2048 Hz, without the need to adjust any hardware or imaging sequences. The algorithm has been validated using a number of qualitative and quantitative measures, including comparison the to the current standard IAR method (Allen et al., 2000). It should be restated that the implementation of IAR used was limited to the available equipment, i.e., the interpolation scheme was not implemented due to the absence of a high-resolution slice-timing signal, resulting in severe residuals. This validation, however, was not intended to assess the general performance of IAR, but rather to compare it to FASTR given a generic, limited setup. Nevertheless, under the assumption that FASTR would produce results similar to IAR after the slice-trigger alignment and average artifact subtraction steps, we have demonstrated that ANC alone would be unable to deal with the residuals on its own, granted that the residuals were probably more severe given the used sampling rate. In addition, the application of the algorithm to simultaneously collected EEG and FMRI data in response to nociceptive stimulation is described in a companion paper (Iannetti et al., this issue). Because of the nature of EEG data and lack of "ground truth" to assess the results against, it is difficult to assess the quality of the EEG using a simple measure. However, we believe that the overall pool of qualitative and quantitative evidence shown provides a solid argument in favor of the quality of EEG that can be achieved.

Although in its current form FASTR cannot be implemented for online artifact removal, it could be modified to suit such a purpose. In a single artifact subtraction step (as opposed to first removing the average then performing PCA/OBS as was described in the Methods section), PCA would be applied to a moving window covering a fixed number of past segments and an OBS calculated from the sample and fitted to the current segment. Alternatively, the same OBS could be used repeatedly and only recalculated when the artifact segments change significantly due to head movement for example. However, this approach could theoretically affect the accuracy of the OBS and its ability to fully explain the artifact variance, as the number of entries used to calculate the OBS is significantly reduced.

Negishi et al. (2004) have proposed an approach for the removal of the gradient artifact similar to the one presented in this paper with few notable differences. Both methods advocate the use of slice-timing correction. In Negishi et al. (2004), after the PCs have been calculated from the contaminated data, the PC scores, their means and standard deviations are calculated for the contaminated data and for data collected without FMRI scanning. For each PC, the ratio of the standard deviation of the PC score for the data without scanning to the standard deviation of the PC score for the contaminated data is used to weight the subtracted projection of the PC from the contaminated data. This procedure has the obvious advantage of avoiding the manual selection of the number of PCs to form an OBS. However, the recording of additional data without scanning is an extra requirement, which could potentially limit the practicality of the experiment. Also, the method proposed by Negishi et al. (2004) assumes that the EEG data collected without scanning is similar in characteristics to the EEG data collected during scanning; an assumption which will not be perfectly correct and could lead to the removal of true EEG information. On the other hand, our proposed approach lacks automatic model order selection, i.e., we do not automatically determined the number of PCs to constitute an OBS. This is a potential area for future improvement. Theoretically, it should be easy to include an automatic selection of the number of components by setting a threshold for the amount of variance to be explained, since the eigenvalue plot of the artifact principal components is quite defined, i.e., there is a clear cut-off for the number of components needed. We do not claim that either our or Negishi's approach is superior. Rather, we see both works as complements that demonstrate the use of temporal PCA in describing and removing residual gradient artifacts and facilitate doing simultaneous EEG and FMRI experiments using a relatively low sampling frequency.

Removing BCG artifacts using subtraction-based methods has also been presented in the literature (Allen et al., 1998; Goldman et al., 2000; Salek-Haddadi et al., 2003; Sijbers et al., 2000). Our approach differs in that it attempts to capture the variation of the artifact in time using the PCA/OBS approach. This approach allows us to not assume the exact same repetition of the artifact (Allen et al., 1998) or assume a simple relationship between occurrences as a function of temporal delay between them (Goldman et al., 2000). It also does not assume a simple scale/amplitude variation of the same basic shape. Rather, the assumption is that over a long enough time, the different BCG artifact occurrences in a single EEG channel are a sample from a constant pool of possible occurrences. The possible variations in this pool can then be explained by the principal components of the samples. We have shown that, on average, this approach decreases the residuals compared to a

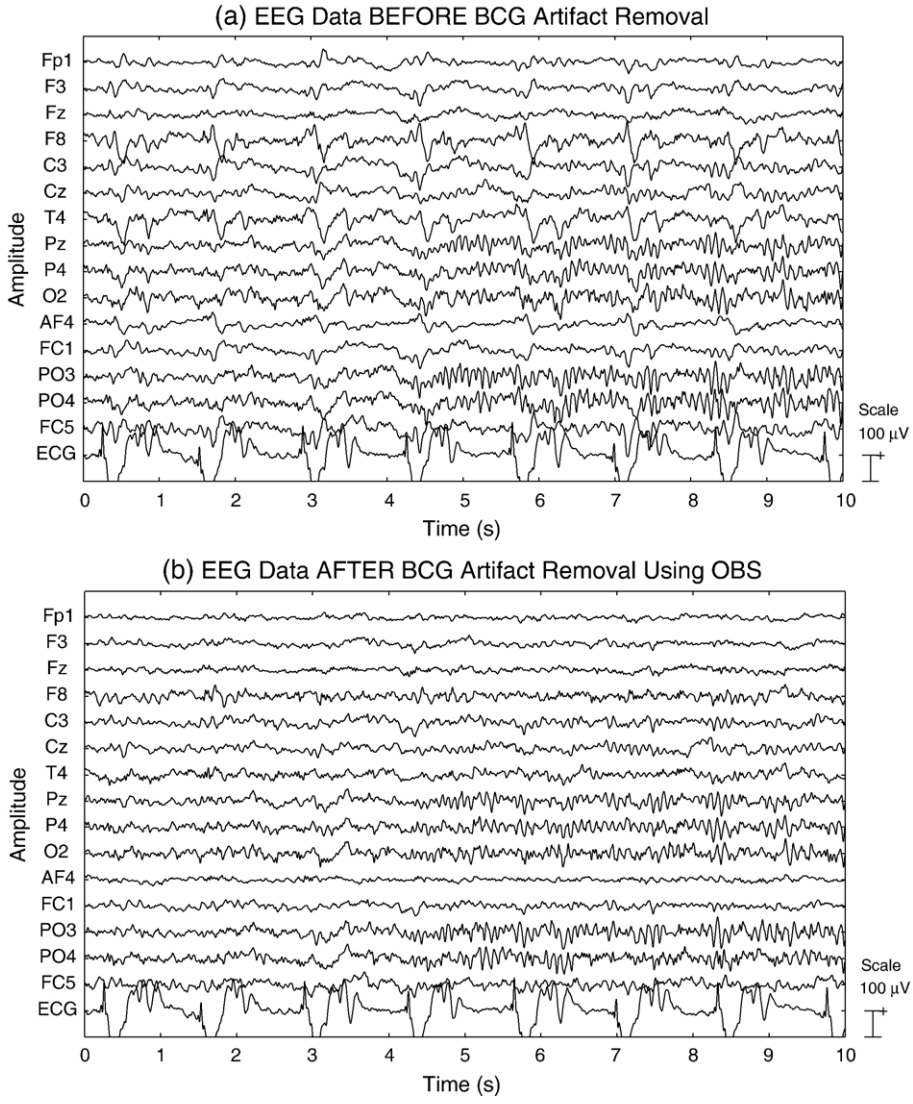

Fig. 14. EEG quality (a) before and (b) after BCG artifact removal using OBS of EEG collected during an eyes opened/eyes closed experiment. The alpha rhythms can clearly be seen in posterior channels starting at approximately 4.5 s when the subject closed his eyes.

simple subtraction method by about 30%. Although the issue of selecting the number of PCs in the OBS is also a concern here. We have found that being conservative and fixing the number of PCs to 3 works well in general. Although Negishi et al. (2004) shed some light on the use of their approach to remove BCG artifacts, they do not compare their results with current approaches and state that more work is needed to fully apply their methods to BCG artifact reduction.

As in any subtraction-based method for BCG artifacts, however, a robust QRS detector is crucial. Implementing a simple thresholding algorithm is not robust to detect QRS peaks as the quality of ECG usually available in EEG systems is not predictable inside the MRI scanner. This is mainly due to movement of electrodes and augmentation of the T wave inside the scanner (Allen et al., 1998; Goldman et al., 2000). We have shown the application of a heuristic algorithm (Christov, 2004) for ECG detection which achieves sensitivity and specificity that rival algorithms applied to multi-lead ECG recordings conducted outside the scanner.

Conclusion

Combining electroencephalography and functional MRI is becoming increasingly important for neuroimaging research. This work presents generic and practical methods to remove FMRI environment-related artifacts from EEG data, which would facilitate the application of this technique to a wide range of settings and applications. Validation of the methods has been provided in this work and in a companion paper (Iannetti et al., this issue) which applied the algorithms described here to a study of simultaneously recorded laser-evoked potentials and FMRI.

Acknowledgments

This work was mainly supported by the Saudi Arabian Cultural Bureau in the UK. This work was also sponsored by the UK Engineering and Physical Sciences Research Council (EPSRC), Pfizer Ltd. and GlaxoSmithKline (GSK) Inc.

References

Allen, P.J., Polizzi, G., Krakow, K., Fish, D.R., Lemieux, L., 1998. Identification of EEG events in the MR scanner: the problem of pulse artifact and a method for its subtraction. NeuroImage 8 (3), 229–239.

Allen, P.J., Josephs, O., Turner, R., 2000. A method for removing imaging artifact from continuous EEG recorded during functional MRI. NeuroImage 12, 230–239.

Anami, K., Mori, T., Tanaka, F., Kawagoe, Y., Okamoto, J., Yarita, M., Ohnishi, T., Yumoto, M., Matsuda, H., Saitoh, O., 2003. Stepping stone sampling for retrieving artifact-free electroencephalogram during functional magnetic resonance imaging. NeuroImage 19 (2 Pt. 1), 281–295.

Bénar, C., Aghakhani, Y., Wang, Y., Izenberg, A., Al-Asmi, A., Dubeau, F., Gotman, J., 2003. Quality of EEG in simultaneous EEG–fMRI for epilepsy. Clin. Neurophysiol. 114 (3), 569–580.

Bonmassar, G., Anami, K., Ives, J., Belliveau, J.W., 1999. Visual evoked potential (VEP) measured by simultaneous 64-channel EEG and 3T fMRI. NeuroReport 10 (9), 1893–1897.

Bonmassar, G., Purdon, P.L., Jaaskelainen, I.P., Chiappa, K., Solo, V., Brown, E.N., Belliveau, J.W., 2002. Motion and ballistocardiogram artifact removal for interleaved recording of EEG and EPs during MRI. NeuroImage 16 (4), 1127–1141.

Christov, I.I., 2004. Real time electrocardiogram QRS detection using combined adaptive threshold. Biomed. Eng. Online 3 (1), 28.

Czisch, M., Wetter, T.C., Kaufmann, C., Pollmacher, T., Holsboer, F., Auer, D.P., 2002. Altered processing of acoustic stimuli during sleep: reduced auditory activation and visual deactivation detected by a combined fMRI/EEG study. NeuroImage 16 (1), 251–258.

Delorme, A., Makeig, S., 2004. EEGLAB: an open source toolbox for analysis of single-trial EEG dynamics including independent component analysis. J. Neurosci. Methods 134 (1), 9–21.

Ellingson, M.L., Liebenthal, E., Spanaki, M.V., Prieto, T.E., Binder, J.R., Ropella, K.M., 2004. Ballistocardiogram artifact reduction in the simultaneous acquisition of auditory ERPS and fMRI. NeuroImage 22 (4), 1534–1542.

Felblinger, J., Slotboom, J., Kreis, R., Jung, B., Boesch, C., 1999. Restoration of electrophysiological signals distorted by inductive effects of magnetic field gradients during MR sequences. Magn. Reson. Med. 41 (4), 715–721.

Garreffa, G., Carni, M., Gualniera, G., Ricci, G.B., Bozzao, L., De Carli, D., Morasso, P., Pantano, P., Colonnese, C., Roma, V., Maraviglia, B., 2003. Real-time MR artifacts filtering during continuous EEG/fMRI acquisition. Magn. Reson. Imaging 21 (10), 1175–1189.

Goldman, R.I., Stern, J.M., Engel Jr., J., Cohen, M.S., 2000. Acquiring simultaneous EEG and functional MRI. J. Clin. Neurophysiol. 111, 1974–1980.

Goldman, R.I., Stern, J.M., Engel, J., Cohen, M.S., 2002. Simultaneous EEG and FMRI of the alpha rhythm. NeuroReport 13 (18), 2487–2492.

Haykin, S., 1986. Adaptive Filter Theory. Prentice-Hall.

Hoffmann, A., Jäger, L., Warhahn, K.J., Jaschke, M., Noachtar, S., Reiser, M., 2000. Electroencephalography during functional echo-planar imaging: detection of epileptic spikes using post-processing methods. Magn. Reson. Med. 44, 791–798.

Iannetti, G.D., Di Bonaventura, C., Pantano, P., Giallonardo, A.T., Romanelli, P.L., Bozzao, L., Manfredi, M., Ricci, G.B., 2002. fMRI/EEG in paroxysmal activity elicited by elimination of central vision and fixation. Neurology 58 (6), 976–979.

Iannetti, G.D., Niazy, R.K., Wise, R.G., Jezzard, P., Brooks, J.C.W., Zambreanu, L., Vennart, W., Matthews, P.M., Tracey, I., this issue. Simultaneous recording of laser-evoked brain potentials and continuous, high-field functional magnetic resonance imaging in humans. Neuroimage. doi:10.1016/j.neuroimage.2005.06.060.

Ives, J.R., Warach, S., Schmitt, F., Edelman, R.R., Schomer, D.L., 1993. Monitoring the patient's EEG during echo planar MRI. Electroencephalogr. Clin. Neurophysiol. 87 (6), 417–420.

Kim, K.H., Yoon, H.W., Park, H.W., 2004. Improved ballistocardiac artifact removal from the electroencephalogram recorded in fMRI. J. Neurosci. Methods 135 (1–2), 193–203.

Krakow, K., Allen, P.J., Symms, M.R., Lemieux, L., Josephs, O., Fish, D.R., 2000. EEG recording during fMRI experiments: image quality. Hum. Brain Mapp. 10 (1), 10–15.

Krakow, K., Messina, D., Lemieux, L., Duncan, J.S., Fish, D.R., 2001. Functional MRI activation of individual interictal epileptiform spikes. NeuroImage 13 (3), 502–505.

Kruggel, F., Wiggins, C.J., Herrmann, C.S., von Cramon, D.Y., 2000. Recording of the event-related potentials during functional MRI at 3.0 Tesla field strength. Magn. Reson. Med. 44 (2), 277–282.

Laufs, H., Kleinschmidt, A., Beyerle, A., Eger, E., Salek-Haddadi, A., Preibisch, C., Krakowa, K., 2003. EEG-correlated FMRI of human alpha activity. NeuroImage 19, 1463–1476.

Lemieux, L., Allen, P.J., Franconi, F., Symms, M.R., Fish, D.R., 1997. Recording of EEG during fMRI experiments: patient safety. Magn. Reson. Med. 38 (6), 943–952.

Lemieux, L., Salek-Haddadi, A., Josephs, O., Allen, P., Toms, N., Scott, C., Krakow, K., Turner, R., Fish, D.R., 2001. Event-related fMRI with simultaneous and continuous EEG: description of the method and initial case report. NeuroImage 14 (3), 780–787.

Liebenthal, E., Ellingson, M.L., Spanaki, M.V., Prieto, T.E., Ropella, K.M., Binder, J.R., 2003. Simultaneous ERP and fMRI of the auditory cortex in a passive oddball paradigm. NeuroImage 19 (4), 1395–1404.

Moosmann, M., Ritter, P., Krastel, I., Brink, A., Thees, S., Blankenburg, F., Taskin, B., Obrig, H., Villringer, A., 2003. Correlates of alpha rhythm in functional magnetic resonance imaging and near infrared spectroscopy. NeuroImage 20, 145–158.

Mukhopadhyay, S., Ray, G.C., 1998. A new interpretation of nonlinear energy operator and its efficacy in spike detection. IEEE Trans. Biomed. Eng. 45 (2), 180–187.

Negishi, M., Abildgaard, M., Nixon, T., Constable, R.T., 2004. Removal of time-varying gradient artifacts from EEG data acquired during continuous fMRI. Clin. Neurophysiol. 115 (9), 2181–2192.

Niazy, R., Iannetti, G., Brady, M., Matthews, P., Smith, S., 2004. A multi-subject study of motor task modulation of EEG-alpha-rhythm/FMRI correlation. Tenth Int. Conf. on Functional Mapping of the Human Brain.

Salek-Haddadi, A., Friston, K.J., Lemieux, L., Fish, D.R., 2003. Studying spontaneous EEG activity with fMRI. Brain Res. Brain Res. Rev. 43 (1), 110–133.

Seeck, M., Michel, C.M., Spinelli, L., Lazeyras, F., 2001. EEG mapping and functional MRI in presurgical epilepsy evaluation. Rev. Neurol. (Paris) 157 (8–9 Pt. 1), 747–751.

Sijbers, J., Van Audekerke, J., Verhoye, M., Van der Linden, A., Van Dyck, D., 2000. Reduction of ECG and gradient related artifacts in simultaneously recorded human EEG/MRI data. Magn. Reson. Imaging 18 (7), 881–886.

Srivastava, G., Crottaz-Herbette, S., Lau, K.M., Glover, G.H., Menon, V., 2005. ICA-based procedures for removing ballistocardiogram artifacts from EEG data acquired in the MRI scanner. NeuroImage 24 (1), 50–60.

Wendt, R.E.r., Rokey, R., Vick, G.W.r., Johnston, D.L., 1988. Electrocardiographic gating and monitoring in NMR imaging. Magn. Reson. Imaging 6 (1), 89–95.